Published in final edited form as:
Magn Reson Med. 2009 March ; 61(3): 587–594. doi:10.1002/mrm.21480.

Investigation of Relationships Between Transverse Relaxation Rate, Diffusion Coefficient, and Labeled Cell Concentration in Ischemic Rat Brain Using MRI

Hemanthkumar Athiraman[1,3], **Quan Jiang**[1,3,*], **Guang Liang Ding**[1], **Li Zhang**[1], **Zheng Gang Zhang**[1], **Lei Wang**[1], **Ali S. Arbab**[2], **Qingjiang Li**[1], **Swayam Panda**[1], **Karen Ledbetter**[1], **Ali M. Rad**[2], and **Michael Chopp**[1,3]

[1]Department of Neurology, Henry Ford Health System, Detroit, Michigan, USA

[2]Department of Radiology, Henry Ford Health System, Detroit, Michigan, USA

[3]Department of Physics, Oakland University, Rochester, Michigan, USA

Abstract

MRI has been used to evaluate labeled cell migration and distribution. However, quantitative determination of labeled cell concentration using MRI has not been systematically investigated. In the current study, we investigated the relationships between labeled cell concentration and MRI parameters of transverse relaxation rate, R_2, and apparent diffusion coefficient (ADC), in vitro in phantoms and in vivo in rats after stroke. Significant correlations were detected between iron concentration or labeled cell concentration and MRI measurements of R_2, ADC, and ADC×R_2 in vitro. In contrast, in vivo labeled cell concentration did not significantly correlate with R_2, ADC, and ADC×R_2. A major factor for the absence of a significant correlation between labeled cell concentration and MRI measurements in vivo may be attributed to background effects of ischemic tissue. By correcting the background effects caused by ischemic damage, ΔR_2 (difference in R_2 values in the ischemic tissue with and without labeled cells) exhibited a significant correlation to labeled cell concentration. Our study suggests that MRI parameters have the potential to quantitatively determine labeled cell concentration in vivo.

Keywords

magnetic resonance imaging; molecular imaging; MRI labeled cells; T_2; diffusion coefficient; stroke

Cell-based therapies have shown promise in the treatment of many neurological diseases including stroke (1-3). Therapeutic benefits may be dependent on the migration and localization of these grafted cells within the target tissue (4,5). Current understanding of migration and quantitative determination of transplanted cells in the host brain has been derived mainly from regional measurements of labeled grafted cells using histological and immunohistological methods (6). However, these methods do not allow dynamic assessment of migration of grafted cells, and only one measurement per experimental animal can be performed. MRI has demonstrated excellent anatomic resolution and specificity via magnetic contrast agents labeled to target cells (5,7-9). Several studies have reported that it

[*]Correspondence to: Quan Jiang, Ph.D., Henry Ford Hospital, Neurology Department, 2799 West Grand Boulevard, Detroit, MI 48202. E-mail: quan@neurnis.neuro.hfh.edu.

is possible to visualize magnetically labeled cells in the brain after transplantation (5,7-9). However, quantitative determination of labeled cells remains a challenge, especially in vivo.

Assessment of brain iron has typically involved the measurement of proton transverse relaxation rate, R_2 (10,11). Several authors have observed a relationship between R_2 and labeled cell concentration in vitro (12). However, the relationship between R_2 and labeled cell concentration is much more complicated in vivo and has not been well studied. Additionally, the theory establishing the relationship between R_2 and labeled cell concentration, especially the effects of diffusion, has not been formulated. In this work, we propose and test a theory relating R_2 and apparent diffusion coefficient (ADC) to labeled cell concentration. Experimental tests were performed both in vitro and in vivo. We demonstrate that R_2, ADC, and ADC×R_2 has a linear relationship with labeled cell concentration in vitro and that multiple factors have to be considered when these relationships are evaluated in vivo, especially the background variation caused by ischemic damage.

THEORY FOR THE RELATIONSHIP BETWEEN R_2, ADC, AND LABELED CELL CONCENTRATION

Evaluating and understanding the performance of magnetic colloids as contrast agents for MRI requires a theory describing their magnetic interactions with water protons. The formulation of outer sphere relaxation of solvent protons by solute particles for $\mu B_0/KT \ll 1$ (μ magnetic moment, B_0 external magnetic field, and K and T are the Boltzmann constant and absolute temperature, respectively) is as follows (13-15):

$$R_2=\left(\frac{32\pi}{405}\right)\gamma_I^2\gamma_S^2\hbar^2\frac{N_A}{1000}\left(\frac{[M]}{rD}\right)\times\{6.5\,j_2(\omega_S)+[1.5\,j_1(\omega_I)+2\,j_1(0)]\} \quad [1]$$

where $\hbar$ is $h/2\pi$, N_A is Avogadro's number, γ_S and γ_I are the gyromagnetic ratios of solute and solvent protons, h is Planck's constant, ω_S and ω_I are the respective Larmor angular precession frequencies of solute and solvent magnetic moments, M is the molarity of solute nanoparticles and j_n the spectral density function (The coefficients of the j_n were derived from the low field limit expressions of $\langle S_{\pm}|$ and $\langle|S_Z|\rangle$, respectively).

The field dependence of the proton longitudinal relaxation rate (nuclear magnetic relaxation dispersion profiles) in aqueous colloidal suspensions of superparamagnetic particles is based on the Curie relaxation, which essentially accounts for the high-field part of the nuclear magnetic resonance dispersion (NMRD) profiles (16). At low fields, one-third of the total mean squared magnetization is found in each of the transverse directions (17). The general equation is

$$R_2=\left(\frac{32\pi}{405}\right)\gamma_I^2\gamma_S^2\hbar^2\quad\frac{N_A}{1000}\left(\frac{[M]}{rD}\right)\times\left\{\begin{array}{c}9.75\left\langle|S_{\pm}|^2\right\rangle j_2(\omega_S)+3\left\langle|Z|^2\right\rangle\\ [1.5\,j_1(\omega_I)+2j_1(0)]\end{array}\right\} \quad [2]$$

After choosing the field strength, and magnetic particles, this formula can be rewritten as,

$$R_2=A\left(\frac{C_{\text{iron}}}{D}\right) \quad [3]$$

$$A=\left(\frac{32\pi}{405}\right)\gamma_I^2\gamma_S^2\hbar^2\left(\frac{1}{r}\right)\times\{9.75\quad\left\langle|S_{\pm}|^2\right\rangle j_2(\omega_S)+3\left\langle|S_z|^2\right\rangle \times\quad[1.5\quad j_1(\omega_I)+2\quad j_1(0)]\} \quad [4]$$

Under the condition of labeled cells having the same iron uptake, $C_{cell} = kC_{iron}$ and k is a constant. The relationship between R_2 and labeled cells will be

$$C_{cell}=\frac{k}{A}DR_2 \quad [5]$$

MATERIALS AND METHODS

The Institutional Animal Care and Use Committee of Henry Ford Hospital have approved all experimental procedures.

In Vitro Study

Phantom Preparation—Ferumoxide suspension contains particles of size 80-150 nm and has original iron concentration of 11.2 mg/ml (Feridex IV; Berlex, Wayne, NJ, USA). Free ferumoxide at different concentrations in 1 ml of phosphate-buffered saline (PBS) were put into NMR tubes (tubes with no magnetic effects) and then 1 ml of liquid 8% gelatin was added to each tube. The solution was mixed thoroughly and quickly (after a short delay to let the bubbles rise) solidified in ice. The final concentrations of ferumoxides were 100, 80, 50, 40, 25, 20, 12.5, 10, 6.25, and 5μg iron/ml, respectively. The NMR tubes were imaged as shown in Fig. 1.

Cell Preparation and Culture—Subventricular zone (SVZ) cells were dissociated along the lateral wall of the lateral ventricle, under the corpus callosum down to the ventral tip of the lateral ventricle from approximately 1.5- to 2.0-mm-thick parasagittal sections from normal male Wistar rats (3-4 months), as previously reported (18). The cells were plated at a density of 2×10^4 cells per milliliter in growth medium. Growth medium contains Dulbecco's modified Eagle's medium (DMEM)-F-12 medium (Invitrogen Corporation, Carlsbad, CA, USA), 20 ng/ml of epidermal growth factor (EGF; R&D Systems, Minneapolis, MN, USA) and basic fibroblast growth factor (bFGF; R&D Systems). DMEM-F-12 medium contains L-glutamine (2 mM), glucose (0.6%), putrescine (9.6 μg/ml), insulin (0.025 mg/ml), progesterone (6.3 ng/ml), apo-transferrin (0.1 mg/ml), and sodium selenite (5.2 ng/ml). The generated neurospheres (primary sphere) were passaged by mechanical dissociation and reseeded as single cells at a density of 20 cells per microliter in EGF-containing media.

Cell Labeling—Cells were labeled with a ferumoxide-protamine sulfate complex (19). Protamine sulfate was prepared as a fresh stock solution in distilled water at the time of use. A ratio of 1 ml: 9μl: 5 μl or 1 ml: 100 μg: 5 μg (serum-free medium: Feridex: protamine sulfate) was mixed and shaken by hand for 5-10 min. Flasks were incubated with Fe complex for 2 h and then 2 ml of fresh media was added to the culture. The SVZ cell suspension was incubated overnight at 37°C in a 5% CO_2 atmosphere to achieve optimal and safe iron loading (12). Four doses of iron (50, 100, 150, and 200 μgFe/ml) were used to test the maximum iron dose that can be used for labeling purposes without altering any properties of the cells used.

The labeled cells were then thoroughly mixed with 8% gelatin solution in NMR tubes. To avoid artifacts due to bubbles, the NMR tubes were left to sit at room temperature for few

minutes until almost all of the bubbles rose up, and then the tubes were solidified in ice. Cell concentrations in NMR tubes ranged from 7.5×10^3 to 2.5×10^6 (per ml). Cells were counted using a hemocytometer.

Cellular Viability—Cell viability was determined by means of trypan blue exclusion. Nonadherent SVZ cells were pipetted up and down approximately 60 times to produce a single-cell suspension. The cells were then mixed with trypan blue dye, and the number of nonstained viable cells to the number of stained nonviable cells was counted.

MRI Studies In Vitro—MRI measurements were performed using a 7T, 20-cm bore superconducting magnet (Magnex Scientific, Abingdon, UK) interfaced to a Bruker console (Billerica, MA, USA). A 12-cm bore actively-shielded gradient coil-set capable of producing magnetic field gradients up to 20 Gauss/cm was used. A homemade birdcage coil was used for all of our in vitro measurements. The imaging protocol consisted of T_2 and diffusion measurements.

Measurement of T_2—T_2 was measured using standard two-dimensional Fourier transform (2DFT) multislice (seven slice) multiecho (six echoes using TE of 7.0, 14.0, 21, 28, 35, and 42 ms MRI with TR of 8 s, 2 averages, 2-mm slice thickness, 32-mm field of view [FOV], 128 × 128 image matrix). The total time for the entire sequence was approximately 34 min.

Measurement of Trace ADC—Trace ADC was measured using the Stejskal-Tanner sequence with three *b*-values (3, 85, and 170 s/mm^2) in each of three diffusion sensitizing directions, seven slices, 2-mm slice thickness, 32 mm FOV, 128 × 128 matrix, TR of 1.5 s, and TE of 19 ms. Each image set for one diffusion sensitizing direction required a scan time of 9 min. The total time for the entire sequence was approximately 27 min.

In vivo study

Cell Labeling—Neural progenitor cells (NPCs) prepared from human fetal brain tissue were provided by Theradigm Inc. Ferumoxide suspension at a concentration of 50 (μg/ml) (with the same ratio as 1 ml: 9 μl: 5 μl of serum-free medium: Feridex: protamine sulfate) was put into a flask containing serum-free RPMI 1640 medium (Biosource, Camarillo, CA, USA) containing 25 mM HEPES (N [2-Hydroxyethyl] piperazine-N' [2-ethanesulfonic acid]), minimal essential medium (MEM), nonessential amino acid, sodium pyruvate, and L-glutamine. Protamine sulfate (American Pharmaceuticals Partner, Schaumburg, IL, USA) at a concentration of 5(μg/ml) was then added to the solution. The solution containing ferumoxide and protamine sulfate was mixed for 5-10 min with intermittent shaking by hand. After 5-10 min, an equal volume of the solution containing ferumoxide and protamine sulfate complexes was added to the cell culture. The cell suspension was then incubated overnight. Prior to injection into the rat, the labeled NPCs were suspended in PBS.

Animal Model and Experiment—Male Wistar rats ($N = 5$) weighing 270-300 g were employed in our experiments. Three hours of middle cerebral artery (MCA) occlusion was induced using a method of intraluminal vascular occlusion. Animals were anesthetized with 3.5% halothane and then maintained with 1.0% to 2.0% halothane in N_2O:O_2 (2:1). Approximately, 1×10^6 NPCs in 1 ml total fluid volume of PBS were injected into the ipsilateral carotid artery 48 h after stroke.

MRI Measurements In Vivo—MRI measurements were performed using a 7T system with a saddle radio frequency (RF) coil as the transmitter and a surface coil as the receiver. Stereotactic ear bars were used to minimize movement during the imaging procedure.

During MRI measurements, anesthesia was maintained using a gas mixture of N_2O (69%), O_2 (30%), and halothane (0.75-1%). Rectal temperature was kept at 37.5°C using a feedback controlled water bath. A tripilot scan of imaging sequence was used for reproducible positioning of the animal in the magnet at each MRI session. MRI measurements, ADC of water (ADC_w), T_2, and three-dimensional (3D) MRI were performed at 1 day before (1 day after onset of stroke) and at 1 and 5 days after cell injection. Animals were killed 5 days after stroke. Ex vivo 3D was performed 1 day after final MRI measurement.

Measurement of Trace ADC—Trace ADC was measured using the Stejskal-Tanner sequence with three *b*-values (20, 600, and 1200 s/mm^2) in each of the three diffusion sensitizing directions, 13 slices, 1-mm slice thickness, 32 mm FOV, 128 × 64 matrix, TR = 1.5 s, and TE = 40 ms. Each direction required a scan time of 4.8 min for completion. The total time for the entire sequence was approximately 14.4 min.

Measurement of T_2—T_2 was measured using standard 2DFT multislice (13 slice) multiecho (six echoes) MRI. A series of four sets of images (13 slices for each set) were obtained using TEs of 15, 30, 45, 60, 75, and 90 ms and a TR of 8 s. Images were produced using a 32 mm FOV, 1-mm slice thickness, and 128 × 64 image matrix. The total time for the entire sequence was approximately 9 min.

3D Measurements—3D gradient echo images were obtained with a TR of 40 ms, TE of 10 ms, 30° flip angle, and a 32 × 32 × 16 mm FOV. The 256 × 192 × 64 voxel matrix was interpolated to 256 × 256 × 64 voxel (0.125 × 0.125 × 0.25 mm) for analysis.

High Resolution Ex Vivo 3D Measurements—3D gradient echo images were obtained with TR of 50 ms, TE of 10 ms, 30° flip angle, 20 × 20 × 10 mm FOV, and 256 × 256 × 128 voxel matrix.

Tissue Preparation and Prussian Blue Staining—Rats were transcardially perfused with heparinized saline and brains were rapidly removed after final MRI measurements 5 days after stroke. The brain was then sliced into 100-μm-thick (Fig. 2a) slices using a vibratome, for analysis of cell number using a 2D confocal microscopic system. To detect Feridex-labeled NPCs in the host brain, brain sections were stained for iron using Prussian blue reaction. The coronal sections were incubated for 30 min with 2% potassium ferro cyanide (Perls' reagent) in 6% HCl, washed, and counterstained with nuclear fast red (10).

Data Analysis

In Vitro Analysis—Raw data were transferred to a Sun station and all image analysis and registration tasks were performed on a Sun UltraSparc 2 workstation (Sun Microsystems Inc., Mountain View, CA, USA) using the Eigentool image analysis software (20). Once the T_2 and ADC maps were produced using Eigentool, the mean values in a region of interest (ROI) located in the center of the tubes were measured.

In Vivo Analysis—To investigate the relationship between R_2, ADC, and labeled cell concentration, MRI and histological images must be carefully coregistered considering the effects from scaling and distortion during histological processing. We first registered 3D sets of images between 3D MRI and histological sections using Eigentool (21) interactive visual observation. Following 3D registration, the 2D images were corrected for distortions and mismatch between MR and histological images. SmartMorph (www.meesoft.com) software was used to warp the histological sections to the corresponding MRI images. Warping is a nonlinear transformation performed at the end of the registration to preserve image quality

and information content. Figure 2 illustrates the process—a histological section (Fig. 2a), a corresponding MR image (Fig. 2b), and a final histology image (Fig. 2c) after coregistration.

ROIs were selected from the dark areas in 3D MRI, which contain labeled cells confirmed by coregistered Prussian blue-stained histology sections. Due to differences in slice thickness between histological section (100 μm), 3D MRI (250 μm), ADC map (1 mm), and T_2 map (1 mm), the largest ROI of the same dark area in the four slices of 3D MRI (1 mm), which corresponds to one slice of T_2 map was used for quantitative measurements of T_2 and ADC values in MRI. Each histological section was 100 μm thick and every fourth slice was used for analysis. Cell numbers obtained from each slide were multiplied by four, accounting for the cells in the saved slices, assuming the distribution to be even.

Considering the possible errors induced by the background differences in ischemic tissues, a correlation analysis considering the background differences was performed. The surrounding nonlabeled cell areas were determined using the areas from 2 to 5 pixels surrounding labeled cell areas (an Eigentool ROI select option). The same anatomic structures (cortex or striatum) with similar ischemic damage as ROIs were used for the comparison purposes. The R_2 difference was calculated by subtraction of R_2 values in the ROI of surrounding nonlabeled cell areas from the corresponding values in the ROI with labeled cells. The changes of relaxivity R_2 were correlated with the labeled cells counted from a histological section in the same volume.

RESULTS

In Vitro Studies

Feridex Labeling of SVZ Cells—Cells were labeled with a ferumoxide-protamine sulfate complex (19). Varying concentrations of superparamagnetic iron oxide (SPIO) particles (0.5-2 mg/ml) were used to determine the maximum concentration of Feridex needed for subsequent cell labeling without any major cell property alterations. After exposure of SVZ cells to ferumoxide-protamine sulfate complex, at a Feridex concentration of 50 μg/ml, >90% of the cells were shown to contain cytoplasmic SPIO particles. Viability of Feridex-labeled SVZ cells were confirmed by trypan blue exclusion and a Live/Dead assay. The test demonstrated that >95% of the labeled SVZ cells were viable. The experiment was repeated three times to confirm the results.

Relationships Between R_2, ADC, ADC×R_2, and Feridex Concentration for Uniform Solution In Vitro—Due to significant signal drop in the diffusion images with high Feridex concentrations, seven reliable ADC data with lower Feridex concentrations (12.5, 8, 10.0, 6.25, 5, 3.125, and 2.5 μg Fe/ml) were used in the study. Figure 3 shows the relationships between R_2 (Fig. 3a), ADC (Fig. 3b), ADC×R_2 (Fig. 3c), and Feridex concentrations. R_2 and ADC×R_2 exhibited a strong linear correlation with Feridex concentrations. The corresponding slopes from linear regression were 0.3542 μg^{-1} S^{-1} ml and 0.4783 μg^{-1} S^{-2} ml mm^2 with r^2 values of 0.9923 and 0.9924, respectively. Unlike the positive relationships between R_2, ADC×R_2, and Feridex concentrations, the ADC decreased as the iron concentration increased. The slopes from linear regression of ADC to Feridex concentration were -0.0436 μg^{-1} S^{-1} ml mm^2 with r^2 values of 0.9338. However, ADC×R_2 further improved the correlation of R_2 with cell concentration as per the theory (Eq. [5]).

Relationships Between R_2, ADC, ADC×R_2, and Labeled Cell Concentration for Uniform Cell Suspension In Vitro—Figure 4 shows the relationships between MRI parameters, R_2 (Fig. 4a), ADC (Fig. 4b), ADC×R_2 (Fig. 4c), and labeled cell concentrations (7.5×10^5 to 2.5×10^6/ml) under in vitro conditions. R_2, ADC, and ADC×R_2 values

exhibited strong linear correlations with cell concentrations. The slopes from linear regression of R_2, ADC, and ADC×R_2 to labeled cell concentration were 10^{-6} S^{-1},10^{-7} ml mm^2, and 10^{-7} S^{-2} ml mm^2 with r^2 values of 0.9932, 0.9517, and 0.9944, respectively. ADC×R_2 further improved the correlation of R_2 with cell concentration.

In Vivo Studies

MRI Appearance of Labeled Cells In Vivo—Figure 5 shows the migration and distribution of labeled cells in the stroked brain in a representative rat. Dark areas in MRI were not detected prior to transplantation of labeled NPCs 1 day after stroke (Fig. 5a). In contrast, the same rat exhibited dark areas at the occipital, parietal, temporal cortex and some in the striatal areas of the ischemic hemisphere at 5 days after injection of labeled cells (Fig. 5b). However, the dark areas in the MRI were rarely detected in the contralateral hemisphere after transplantation (Fig. 5b). The ex vivo 3D images (Fig. 5c and d) from the same animal with high resolution exhibited additional details of the distribution of labeled cells in the ischemiadamaged region. Consistent with MRI observations, the Prussian blue staining sections (Fig. 5e and f) obtained 5 days after cell transplantation showed clusters of positive Prussian blue-stained labeled cells (Fig. 5e, black-boxed area; arrows in Fig. 5f mark that same boxed area in the magnified Prussian blue-stained image) in the ischemic lesion.

Correlations Between R_2, ADC, ADC×R_2, and the Number of Labeled Cell Concentration In Vivo—Figure 6 shows the relationships between R_2 (Fig. 6a), ADC (Fig. 6b), ADC×R_2 (Fig.6c), and labeled cell concentrations in living rat brain. There were no correlations between ADC, ADC×R_2, and labeled cell concentration in vivo, while R_2 showed a moderate correlation. The slopes from linear regression of R_2, ADC, and ADC×R_2 to labeled cell concentration were 0.0037 S^{-1}ml, -0.0041 S^{-1}mlmm^{2}and 0.0018 S^{-2}mlmm^2 with r^2 values of 0.5489, 0.1817, and 0.2689 respectively.

Correlations Between R_2 and Labeled Cell Concentration In Vivo After Considering Background Differences—To correct the effects of background tissue differences on the relationship between R_2 and labeled cell concentration, the R_2 differences (ΔR_2) were calculated by subtraction of R_2 values in the surrounding nonlabeled cell ROI from the values in the corresponding ROI with labeled cells. The correlation between ΔR_2 and labeled cell concentration improved significantly compared to that without background correction (Fig. 6d). The slope from linear regression of the changes of ΔR_2 and labeled cell concentration was 0.0238 S^{-1} ml with r^2 values of 0.9086. ΔR_2×ADC + R_2×ΔADC vs. iron concentration was measured but had no significant correlation.

DISCUSSION

In this study, we have investigated the effects of MRI parameters, R_2 and ADC, on the labeled cell concentration both in vitro and in vivo conditions. MRI parameters, R_2, ADC, and ADC×R_2, showed significant correlations to iron-labeled cell concentration, and considering diffusion effects improved the correlation between labeled cell concentration and transverse relaxivity, as predicted in theory under in vitro conditions but not in vivo. However, by correcting the background variation in vivo, the R_2 differences, ΔR_2, exhibited an improved correlation to labeled cell concentration. Our study demonstrated that MRI could be used to evaluate labeled cell concentration both in vitro and in vivo.

Brain tissue iron concentration has been assessed by the measurement of proton R_2 (22-24). Several authors have observed a relationship between R_2 and iron levels (11,12,22-24). However, there is no mathematical expression for the relationship between MRI

measurements and labeled cell concentration. The changes of diffusion constant influence the relationship between labeled cell concentration and R_2 value (28-30). An increase in the magnitude or range of local magnetic field gradients can decrease the ADC value (25). Changes in local magnetic field gradients can be induced either by a paramagnetic contrast agent or labeled cells. It can be argued that the ADC×R_2 images would be better than R_2 to evaluate iron concentration. Compared with R_2 alone, ADC×R_2 exhibits an improved correlation in both labeled cell and iron concentration in vitro but not in vivo after stroke. The inconsistency between the theory and in vivo experimental results may result from a diffusion effect on iron concentration, measurement errors, and background variation of MRI measurements in ischemia-damaged tissue. The changes of ADC are relatively small with iron concentration. Based on in vitro studies of labeled cell concentration and ADC (Fig. 4), the change in ADC from in vivo data is 3.5×10^{-5} mm^2/s for the highest cell concentration (2.5×10^6/ml; Fig. 6). However, the changes in ADC caused by labeled cells are much smaller than that induced by ischemic damage. In cat and rat ischemic models, ADC decreases 30% to 60% (approximately 3×10^{-4} mm^2/s), reaches a maximum decrease at about 24 h (26-31) and becomes elevated above control levels 48 h after onset of stroke (27-29,32). The degree of decrease in ADC also depends on the anatomic location of the ischemic lesion (28,29). The large heterogeneous variation of ADC after stroke makes the investigation of the correlation between ADC and labeled cell concentration difficult. However, ADC effects on labeled concentration could be considered as a constant in Eq. [5] because of the relatively small variation of ADC caused by labeled cells.

The large variation of T_2 after stroke also affects quantitative evaluation of labeled cell concentration. T_2 exhibits a delayed increase compared to ADC and reaches a maximum at 24 - 48 h (approximately 70%) after stroke in animals (28,29). T_2 changes also depend on the anatomic location of ischemic lesion (28,29,33). Therefore, it is impossible to get an accurate evaluation for the relationships between MRI parameters and labeled cell concentration without considering background variation caused by ischemic damage. Our in vivo data demonstrate that there are no correlations between ADC, ADC×R_2, and labeled cell concentration, and R_2 showed a moderate correlation if the background variation was not considered. By correcting ischemic induced changes in MRI parameters, the R_2 difference exhibited a significant correlation to labeled cell concentration. Our results demonstrated that ΔR_2 is a useful parameter to evaluate labeled cell concentration in vivo.

There are several other factors, such as cell proliferation and label dilution, cell death, macrophage effects, local magnetic field variation, etc., that need to be considered for a complete in vivo evaluation of cell concentration. Cell proliferation and label dilution will effect the determination of labeled cell concentration using relaxivities in vivo (34). It has been shown that over time with cell divisions their is a constant decrease in labeled particles (35). The decreases in the iron per cell after cell proliferation will reduce the slope of the curve of relaxivity vs. labeled cell concentration (12,36). Also, cell proliferation will be affected by the localized microenvironment, i.e., the proliferation will be slow in the ischemic core and faster in the ischemic boundary. However, our experiment has been designed to minimize these effects by sacrificing animals early after labeled cell migration into ischemic brain (37). Further study is needed to investigate the relationship of MRI measurements and labeled cell concentration with cell proliferation, label dilution, cell death, macrophage effects, etc. under conditions of extended monitoring time.

In conclusion, our data indicate that the effects of diffusion coefficient on the evaluation of labeled cell concentration are relatively small, although its involvement is clearly demonstrated. The ADC×R_2 theory is only confirmed under relatively low iron-loading conditions in an in vitro labeled cell study with minimized background effects. By correcting background effects, ΔR_2 provides an index for the evaluation of labeled cell

concentration in vivo. Our study suggests that MRI parameters have the potential to quantitatively determine labeled cell concentration in vivo.

Acknowledgments

We thank Smita Savant-Bhonsale and Padmavathy Vanguri (Theradigm Inc., Baltimore, MD, USA) for providing cells for our studies. We also thank Polly Whitton for her editorial work.

Grant sponsor: National Institutes of Health (NIH); Grant numbers: RO1 NS48349; NS38292; NS43324; HL64766; PO1 NS23393; NS42345; Mort and Brigitte Harris Foundation.

REFERENCE

1. Bang OY, Lee JS, Lee PH, Lee G. Autologous mesenchymal stem cell transplantation in stroke patients. Ann Neurol. 2005; 57:874–882. [PubMed: 15929052]
2. Chopp M, Li Y. Treatment of neural injury with marrow stromal cells. Lancet Neurol. 2002; 1:92–100. [PubMed: 12849513]
3. Zhang R, Zhang Z, Wang L, Wang Y, Gousev A, Zhang L, Ho KL, Morshead C, Chopp M. Activated neural stem cells contribute to stroke-induced neurogenesis and neuroblast migration toward the infarct boundary in adult rats. J Cereb Blood Flow Metab. 2004; 24:441–448. [PubMed: 15087713]
4. Dunnett SB, Bjorklund A, Lindvall O. Cell therapy in Parkinson's disease—stop or go? Nat Rev Neurosci. 2001; 2:365–369. [PubMed: 11331920]
5. Jiang Q, Zhang ZG, Ding GL, Zhang L, Ewing JR, Wang L, Zhang R, Li L, Lu M, Meng H, Arbab AS, Hu J, Li QJ, Pourabdollah Nejad DS, Athiraman H, Chopp M. Investigation of neural progenitor cell induced angiogenesis after embolic stroke in rat using MRI. Neuroimage. 2005; 28:698–707. [PubMed: 16112879]
6. Auerbach JM, Eiden MV, McKay RD. Transplanted CNS stem cells form functional synapses in vivo. Eur J Neurosci. 2000; 12:1696–1704. [PubMed: 10792447]
7. Bulte JW, Zhang S, van Gelderen P, Herynek V, Jordan EK, Duncan ID, Frank JA. Neurotransplantation of magnetically labeled oligodendrocyte progenitors: magnetic resonance tracking of cell migration and myelination. Proc Natl Acad Sci USA. 1999; 96:15256–15261. [PubMed: 10611372]
8. Jiang Q, Ewing JR, Ding GL, Zhang L, Zhang ZG, Li L, Whitton P, Lu M, Hu J, Li QJ, Knight RA, Chopp M. Quantitative evaluation of BBB permeability after embolic stroke in rat using MRI. J Cereb Blood Flow Metab. 2005; 25:583–592. [PubMed: 15716859]
9. Zhang ZG, Jiang Q, Zhang L, Wang L, Zhang L, Arniego P, Ho KL, Chopp M. Magnetic resonance imaging and neurosphere therapy of stroke in rat. Ann Neurol. 2003; 53:259–63. [PubMed: 12557295]
10. Bizzi A, Brooks RA, Brunetti A, Hill JM, Alger JR, Miletich RS, Francavilla TL, Di Chiro G. Role of iron and ferritin in MR imaging of the brain: a study in primates at different field strengths. Radiology. 1990; 177:59–65. [PubMed: 2399339]
11. Vymazal J, Brooks RA, Patronas N, Hajek M, Bulte JW, Di Chiro G. Magnetic resonance imaging of brain iron in health and disease. J Neurol Sci. 1995; 134(Suppl):19–26. [PubMed: 8847541]
12. Zelivyanskaya ML, Nelson JA, Poluektova L, Uberti M, Mellon M, Gendelman HE, Boska MD. Tracking superparamagnetic iron oxide labeled monocytes in brain by high-field magnetic resonance imaging. J Neurosci Res. 2003; 73:284–295. [PubMed: 12868062]
13. Pfeiffer H. Der Translationsanteil der protonenrelaxation in wasserigen Losungen paramagnetischen Ionen. Ann Phys (Leipzig). 1961; 8:1–8.
14. Hwang L-P. Dynamic effects of pair correlation functions on spin relaxation by translational diffusion in liquids. J Chem Phys. 1975; 63:4017–4025.
15. Freed JH. Dynamic effects of pair correlation functions on spin relaxation by translational diffusion in liquids. II. Finite jumps and independent T1 processes. J Chem Phys. 1978; 68:4034–4037.

16. Koenig SH. From the relaxivity of Gd(DTPA)2- to everything else. Magn Reson Med. 1991; 22:183–190. [PubMed: 1812344]

17. Koenig SH, Kellar KE. Theory of 1/T1 and 1/T2 NMRD profiles of solutions of magnetic nanoparticles. Magn Reson Med. 1995; 34:227–233. [PubMed: 7476082]

18. Morshead CM, Reynolds BA, Craig CG, McBurney MW, Staines WA, Morassutti D, Weiss S, van der Kooy D. Neural stem cells in the adult mammalian forebrain: a relatively quiescent subpopulation of subependymal cells. Neuron. 1994; 13:1071–1082. [PubMed: 7946346]

19. Arbab AS, Yocum GT, Kalish H, Jordan EK, Anderson SA, Khakoo AY, Read EJ, Frank JA. Efficient magnetic cell labeling with protamine sulfate complexed to ferumoxides for cellular MRI. Blood. 2004; 104:1217–1223. [PubMed: 15100158]

20. Windham JP, Abd-Allah MA, Reimann DA, Froelich JW, Haggar AM. Eigenimage filtering in MR imaging. J Comput Assist Tomogr. 1988; 12:1–9. [PubMed: 3335646]

21. Jacobs MA, Knight RA, Soltanian-Zadeh H, Zheng ZG, Goussev AV, Peck DJ, Windham JP, Chopp M. Unsupervised segmentation of multiparameter MRI in experimental cerebral ischemia with comparison to T2, diffusion, and ADC MRI parameters and histopathological validation. J Magn Reson Imaging. 2000; 11:425–437. [PubMed: 10767072]

22. Alexopoulou E, Stripeli F, Baras P, Seimenis I, Kattamis A, Ladis V, Efstathopoulos E, Brountzos EN, Kelekis AD, Kelekis NL. R2 relaxometry with MRI for the quantification of tissue iron overload in beta-thalassemic patients. J Magn Reson Imaging. 2006; 23:163–170. [PubMed: 16374880]

23. Gelman N, Gorell JM, Barker PB, Savage RM, Spickler EM, Windham JP, Knight RA. MR imaging of human brain at 3.0 T: preliminary report on transverse relaxation rates and relation to estimated iron content. Radiology. 1999; 210:759–767. [PubMed: 10207479]

24. Gossuin Y, Muller RN, Gillis P. Relaxation induced by ferritin: a better understanding for an improved MRI iron quantification. NMR Biomed. 2004; 17:427–432. [PubMed: 15526352]

25. Jianhui Z. Effects of susceptibility variations on NMR measurements of diffusion. J Magn Reson. 1991; 95:267–280.

26. Jiang N, Kowaluk EA, Lee CH, Mazdiyasni H, Chopp M. Adenosine kinase inhibition protects brain against transient focal ischemia in rats. Eur J Pharmacol. 1997; 320:131–137. [PubMed: 9059845]

27. Jiang Q, Chopp M, Zhang ZG, Helpern JA, Ordidge RJ, Ewing J, Jiang P, Marchese BA. The effect of hypothermia on transient focal ischemia in rat brain evaluated by diffusion- and perfusion-weighted NMR imaging. J Cereb Blood Flow Metab. 1994; 14:732–741. [PubMed: 8063869]

28. Jiang Q, Zhang ZG, Chopp M, Helpern JA, Ordidge RJ, Garcia JH, Marchese BA, Qing ZX, Knight RA. Temporal evolution and spatial distribution of the diffusion constant of water in rat brain after transient middle cerebral artery occlusion. J Neurol Sci. 1993; 120:123–130. [PubMed: 8138799]

29. Knight RA, Ordidge RJ, Helpern JA, Chopp M, Rodolosi LC, Peck D. Temporal evolution of ischemic damage in rat brain measured by proton nuclear magnetic resonance imaging. Stroke. 1991; 22:802–808. [PubMed: 2057981]

30. Moseley ME, Cohen Y, Mintorovitch J, Chileuitt L, Shimizu H, Kucharczyk J, Wendland MF, Weinstein PR. Early detection of regional cerebral ischemia in cats: comparison of diffusion- and T2-weighted MRI and spectroscopy. Magn Reson Med. 1990; 14:330–346. [PubMed: 2345513]

31. Moseley ME, Kucharczyk J, Mintorovitch J, Cohen Y, Kurhanewicz J, Derugin N, Asgari H, Norman D. Diffusion-weighted MR imaging of acute stroke: correlation with T2-weighted and magnetic susceptibility-enhanced MR imaging in cats. AJNR Am J Neuroradiol. 1990; 11:423–429. [PubMed: 2161612]

32. Jiang Q, Chopp M, Zhang ZG, Knight RA, Jacobs M, Windham JP, Peck D, Ewing JR, Welch KM. The temporal evolution of MRI tissue signatures after transient middle cerebral artery occlusion in rat. J Neurol Sci. 1997; 145:15–23. [PubMed: 9073024]

33. Jiang Q, Zhang ZG, Ding GL, Silver B, Zhang L, Meng H, Lu M, Pourabdillah-Nejed DS, Wang L, Savant-Bhonsale S, Li L, Bagher-Ebadian H, Hu J, Arbab AS, Vanguri P, Ewing JR, Ledbetter

KA, Chopp M. MRI detects white matter reorganization after neural progenitor cell treatment of stroke. Neuroimage. 2006; 32:1080–1089. [PubMed: 16860575]

34. Daldrup-Link HE, Rudelius M, Oostendorp RA, Settles M, Piontek G, Metz S, Rosenbrock H, Keller U, Heinzmann U, Rummeny EJ, Schlegel J, Link TM. Targeting of hematopoietic progenitor cells with MR contrast agents. Radiology. 2003; 228:760–767. [PubMed: 12881578]
35. Hinds KA, Hill JM, Shapiro EM, Laukkanen MO, Silva AC, Combs CA, Varney TR, Balaban RS, Koretsky AP, Dunbar CE. Highly efficient endosomal labeling of progenitor and stem cells with large magnetic particles allows magnetic resonance imaging of single cells. Blood. 2003; 102:867–872. [PubMed: 12676779]
36. Bowen CV, Zhang X, Saab G, Gareau PJ, Rutt BK. Application of the static dephasing regime theory to superparamagnetic iron-oxide loaded cells. Magn Reson Med. 2002; 48:52–61. [PubMed: 12111931]
37. Zhang R, Wang L, Zhang L, Chen J, Zhu Z, Zhang Z, Chopp M. Nitric oxide enhances angiogenesis via the synthesis of vascular endothelial growth factor and cGMP after stroke in the rat. Circ Res. 2003; 92:308–313. [PubMed: 12595343]

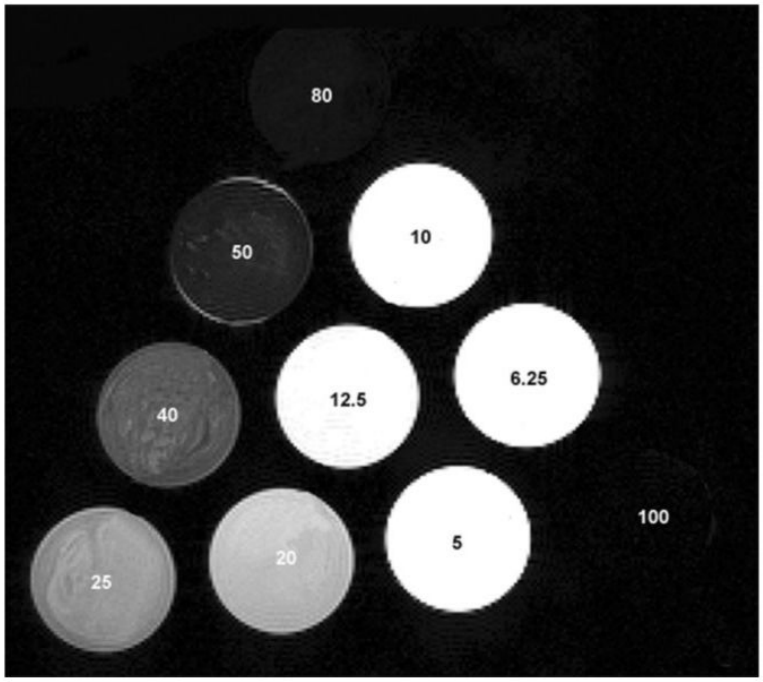

FIG. 1.

Feridex concentrations were varied to investigate the relationships between MRI measurements and iron concentration in gel phantoms at 7T. T_2 and ADC maps were obtained using 5-mm NMR tubes containing different Feridex concentrations (as marked on the tubes with units of μg Fe/ml).

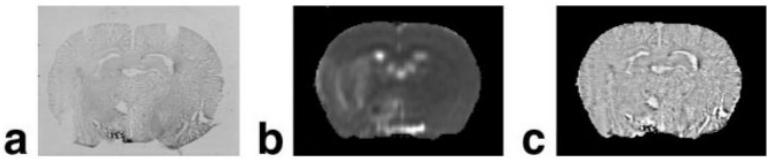

FIG. 2.

Coregistration of MRI and histology. Histological sections were coregistered and warped to MRI images of ischemic rat brain. **a:** Histological section before processing (warping, scaling, etc). **b:** T_2 MR image used as reference for processing the corresponding histological section. **c:** Histological section after coregistration and warping.

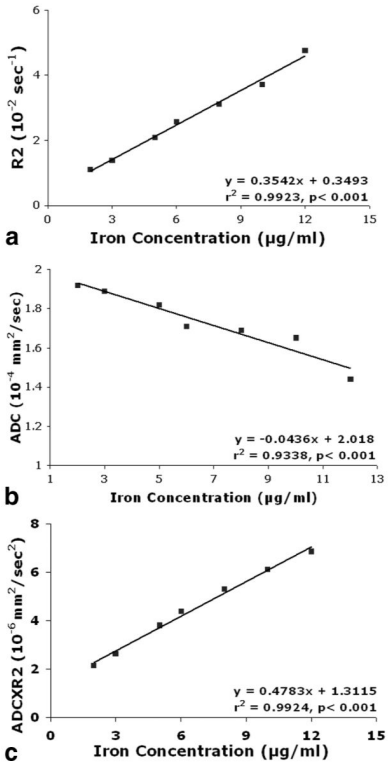

FIG. 3.

Graphs showing R_2 (**a**), ADC (**b**), and ADC×R_2 (**c**) values measured in gelatin phantoms. Relaxation rates are shown as a function of Feridex concentration. The R_2 (**a**) and ADC×R_2 (c) exhibited a significant positive linear correlation while ADC×R_2 (c) improved the positive correlation and ADC (b) showed a negative linear correlation.

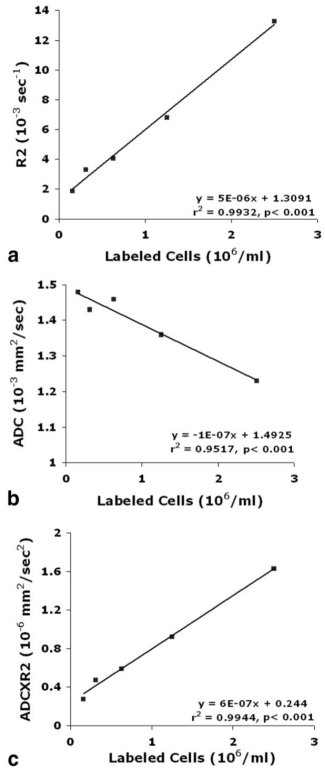

FIG. 4.

Graphs showing the relationships between R_2 (**a**), ADC (**b**), and ADC×R_2 (**c**) and labeled cell concentration in gelatin phantoms. The R_2 (**a**) and ADC (**b**) exhibited significant correlations with labeled cell concentration, and ADC×R_2 (**c**) further improved the correlation with labeled cell concentration.

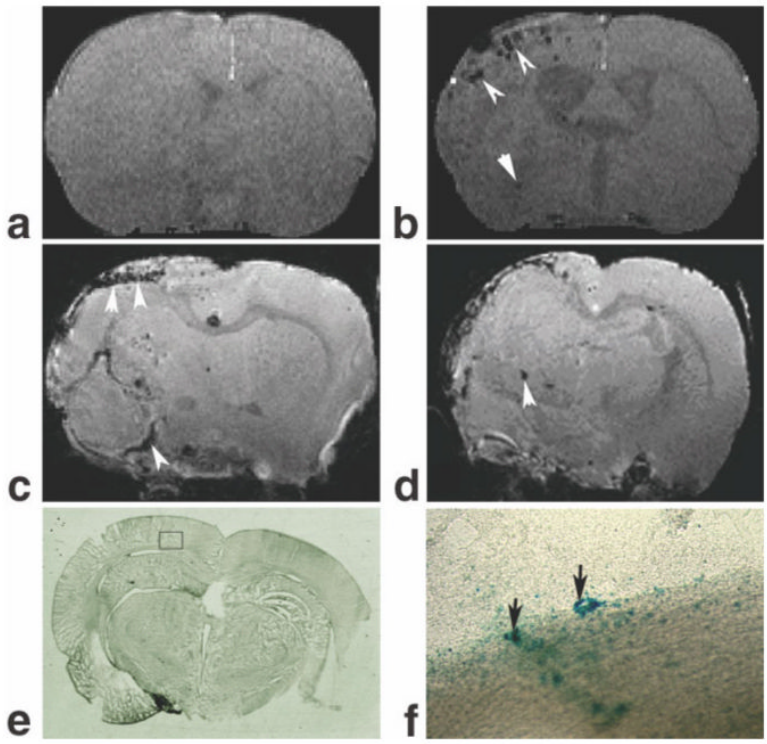

FIG. 5.

Labeled cell appearances in gradient echo 3D images from ischemic rat brain at 1 day before (**a**) and 5 days after (**b**) transplantation of labeled cells, and the corresponding ex vivo images (**c,d**) from the same rat. The dark areas caused by labeled cells in the 3D MRI were not detected before transplantation of labeled cells (a). In contrast, the same rat exhibited the dark areas in ischemic boundary at 5 days after injection of labeled cells (b). The ex vivo 3D images (c,d) with high resolution exhibited additional details of the distribution of labeled cells in the ischemic damaged region. The Prussian blue staining sections (**e,f**) obtained from the same rat 5 days after transplantation showed clusters of Prussian blue-positive cells indicating Feridex-labeled cells (black box area (e); black arrows in the magnified image (f) from the box in (e)) in the ischemic boundary.

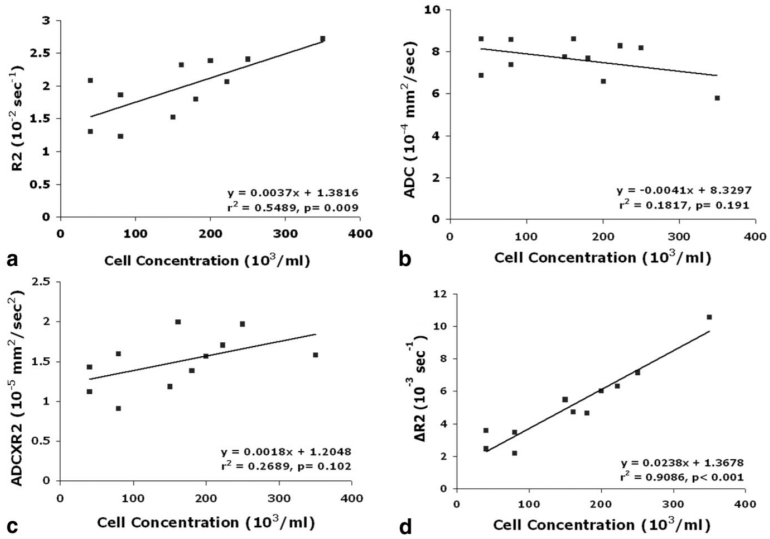

FIG. 6.

Graphs showing the relationships between R_2 (**a**), ADC (**b**), ADC×R_2 (**c**), ΔR_2 (**d**), and labeled cell concentration in vivo. ADC (b) and ADC×R_2 (c) did not exhibit significant correlation with labeled cell concentration while R_2 (a) showed a moderate correlation. However, ΔR_2 (d) showed significant correlation with labeled cell concentration after correcting background variation.